



Interaction between the magnetic and superconducting order parameters in a $\text{La}_{1.94}\text{Sr}_{0.06}\text{CuO}_4$ wire studied via muon spin rotation

Meni Shay, Amit Keren, Gad Koren, Amit Kanigel, Oren Shafir, and Lital Marcipar
Department of Physics, Technion-Israel Institute of Technology, Haifa 32000, Israel

Gerard Nieuwenhuys, Elvezio Morenzoni, Andreas Suter, and Thomas Prokscha
Paul Scherrer Institute, CH 5232 Villigen PSI, Switzerland

Moshe Dubman

Paul Scherrer Institute, CH 5232 Villigen PSI, Switzerland and Institut für Physik der Kondensierten Materie, TU Braunschweig, D-38106 Braunschweig, Germany

Daniel Podolsky

Department of Physics, University of Toronto, Toronto, Ontario, Canada M5S 1A7

(Received 30 July 2009; revised manuscript received 4 September 2009; published 7 October 2009)

We investigate the coupling between the magnetic and superconducting order parameters in an 8-m-long meander line (“wire”) made of a $\text{La}_{1.94}\text{Sr}_{0.06}\text{CuO}_4$ film with a cross section of $0.5 \times 100 \mu\text{m}^2$. The magnetic order parameter is determined using the low-energy muon spin relaxation technique. The superconducting order parameter is characterized by transport measurements and modified by high current density. We find that when the superconducting order parameter is suppressed by the current, the magnetic transition temperature, T_m , increases. The extracted sign and magnitude of the Ginzburg-Landau coupling constant indicate that the two orders are repulsive, and that our system is located close to the border between first- and second-order phase transition.

DOI: [10.1103/PhysRevB.80.144511](https://doi.org/10.1103/PhysRevB.80.144511)

PACS number(s): 74.78.Bz, 74.25.Ha, 74.72.-h

I. INTRODUCTION

When cuprates are doped their low-temperature ordered phase changes from an antiferromagnetic (AFM) to a superconducting (SC) one. The transition takes place over a range of doping levels where, at low enough temperatures, the samples are both superconducting and magnetic.¹⁻³ It is natural to expect phase separation due to the inhomogeneous doping. However, a local probe such as muon spin relaxation indicates that the magnetic volume fraction is 100%, namely, the magnetic field exists everywhere, even in the SC regions.¹ Therefore, the nature of the presence of SC and magnetism is puzzling. What is the order of the transition between the AFM and SC phases as a function of doping? Is it first order with phase separation or second order with coexistence? Are the two orders coupled, and if yes, what are the sign and strength of the coupling?

Here we answer these questions by looking at the effect of current I on the magnetic phase transition temperature, T_m . A current, on the scale of the second critical current I_{c2} , diminishes the superconducting order parameter. If the two orders interact, the magnetic order parameter is expected to react to the current and either increase or decrease depending on the type of coupling between the two orders. This, in turn, will increase or decrease T_m , respectively. Therefore, we map the magnetic phase transition with and without current. Our major finding in this work is that with current of about $0.2I_{c2}$ the magnetic phase transition temperature increases. This is shown in Fig. 1. It implies that the orders are coupled repulsively. Analysis based on the Ginzburg-Landau (GL) model shows that the phase transition between AFM and SC must be close to the border between first and second order.

II. EXPERIMENT

A. Sample preparation and characterization

The experiment is done with an 8-m-long wire made of $\text{La}_{1.94}\text{Sr}_{0.06}\text{CuO}_4$ film. The inset of Fig. 2 shows a magnified image of one corner of the sample. The film is prepared using laser ablation deposition on (100) LaAlO_3 substrate, standard photolithographic patterning, and wet acid etching (0.05% HCl). The length of the wire is set by the experimental requirements discussed in Sec. II B. The 6% Sr doping was chosen since the corresponding bulk material has a $T_c \approx 10$ K and $T_m \approx 6$ K,^{1,4,5} which makes both critical temperatures reachable in a standard cryostat. The height of the

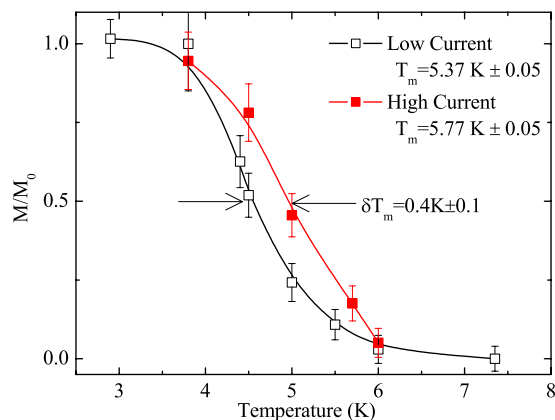


FIG. 1. (Color online) The magnetic phase transition without current and with high current $\sim 0.2I_{c2}$. Solid lines are guides to the eye.

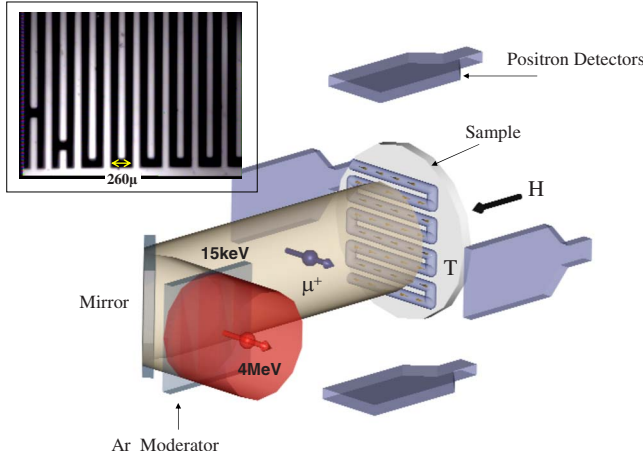


FIG. 2. (Color online) A schematic visualization of the experiment. The high-energy muon beam is slowed down by an argon moderator and the slow muons are stopped in the thin wire. The wire is folded into a meander line so that the muon beam covers the whole wire. Top left inset: a magnified image of part of the wire.

wire is $0.5 \mu\text{m}$ and is selected so that one of the dimensions of the wire is on the order of the penetration depth. This ensures that current flows in the bulk of the wire. The cross section of the wire is $0.5 \mu\text{m} \times 100 \mu\text{m}$ so that a typical applied current of a few mA is comparable to I_{c2} . The last two points are further discussed in Secs. III B and III D, respectively. Finally, the sample was found to be a bulk superconductor as shown in Sec. III B.

B. Low energy μSR

Probing the magnetic properties of such a thin wire is achieved by using the low-energy muon spin relaxation (LE- μSR) technique.^{6,7} A schematic representation of the experimental setup is shown in Fig. 2. In this technique, the muons are first slowed down in an Ar moderator where their kinetic energy drops from 4 MeV to 15 eV, while their initial full polarization is conserved. They are then electrostatically accelerated to 15 keV and transported using an electrostatic mirror to the sample in ultrahigh vacuum (UHV). Four counters collect positrons from the asymmetric muon decay. One pair of counters, known as forward (F) and backward (B), collect positrons emitted parallel or antiparallel to the initial muon spin direction. The other pair, known as up (U) and down (D), collect positrons emitted perpendicular to it. The muon asymmetry in these directions is calculated by taking the difference over the sum of the count for each pair, namely,

$$A_z(t) = \frac{B(t) - F(t)}{B(t) + F(t)}, \quad A_\perp(t) = \frac{U(t) - D(t)}{U(t) + D(t)}, \quad (1)$$

where \hat{z} is the initial muon spin direction once it enters the sample. This asymmetry is proportional to the component of the muon polarization in each direction: $P_z(t) \propto A_z(t)$ and $P_\perp(t) \propto A_\perp(t)$.

The field the muon experiences is either internal, below T_m , or external (designated by H), or both. For more details

on μSR in the presence of superconductivity and magnetism see Ref. 8. The muons beam spot size has a 15 mm diameter (full width at half maximum). In order to avoid muons missing the sample, the wire is folded in the form of a long meandering line covering a disk 3 cm in diameter.

C. Temperature measurement

The temperature of the sample is measured in a nontrivial way using a calibration that makes use of the sample as its own thermometer. Such a procedure is required since the sample is in a UHV ambient and it is cooled by a cold finger. Although a Cernox thermometer is attached to the cold finger, it delivers the temperature of the sample only at very low currents. This happens because above the first critical current, I_{c1} , the superconducting wire acts as a heater and it is not in thermal equilibrium with either the cold finger or any attached thermometer. Therefore, the wire's temperature can be measured only by an *a priori* calibration procedure in a flow cryostat with He ambient. In such a cryostat the thermal contact between the wire and a thermometer, even at high currents, is good. In the calibration procedure the voltage drop on the wire is determined for each temperature and current using standard dc four-probe measurement. The probes are attached to the sample using silver paste and the measurement is done with a KEITHLEY 2400 Sourcemeter. The temperature is measured using a calibrated Cernox thermometer and an Oxford ITC501 controller. About 100 data points of voltage and temperature are taken in intervals of a few seconds. The statistics of these data points is used to produce the calibration shown in left-hand side of Table I.

In the LE- μSR experiment the calibration is used in the following way: we choose the desired current and temperature for a run. The cold finger is set to a temperature close to the desired temperature, then the current is applied to the sample. The voltage on the sample is measured again using four probes, as in the calibration procedure. Then the cold finger temperature is lowered until the voltage on the sample matches the calibrated value for the desired temperature and current. During the LE- μSR run, the voltage across the wire is measured in intervals of a few seconds, to produce the average voltage and its standard deviation. Using the calibration table this voltage is translated to temperature. This translation is shown, for each run, in the right-hand side of Table I. To account for possible drifts we repeated the calibration in the flow cryostat also after the LE- μSR experiment. It was found that the V - I - T values did not change in the 3 weeks time interval in which the calibration and experiment were done. This proved the temperature uncertainty to be smaller than 0.01 K, namely, the temperature difference between two runs at the same desired temperature is smaller than 0.01 K.

D. Transport

The normal-state resistivity of the wire was measured over different segments of the wire to ensure that it is evenly distributed and that there are no weak links. The sample was also examined under a microscope and no shorts between neighboring lines of the wire or obvious inhomogeneities were found. The critical current I_{c1} where voltage first starts

TABLE I. Temperature calibration table.

T (K)	ΔT (mK)	I (mA)	V (V)	ΔV (mV)	$\Delta V/\Delta T$ (V/K)	$V@_{\mu\text{SR}}$ (V)	ΔV (mV)	$T@_{\mu\text{SR}}$ (K)	ΔT (mK)	Symbol in Fig. 3
3.800	1	0.5	0.0506	0.01	0.01	0.0504	0.1	3.785	10	○
3.80	30	5	11.5	100	3	11.5	200	3.81	60	●
4.499	2	0.5	0.07505	0.07	0.03	0.0751	0.4	4.501	12	
4.501	2	4.3	9.93	10	0.7	9.936	23	4.507	4	
4.999	1	0.5	0.1043	0.1	0.04	0.1045	0.4	5.004	4	-□-
4.995	5	4	10.63	40	6	10.68	100	5.005	10	-■-
5.500	1	0.5	0.1438	0.2	0.06	0.1438	0.2	5.500	1	
5.506	3	3.5	10.09	20	2	10.62	60	5.7	10	
5.999	2	0.5	0.19271	0.2	0.1	0.1927	0.4	5.999	4	
5.994	2	3	9.38	10	5	9.43	40	6.003	8	
7.35	10	0.5	0.395	1	0.2	0.3963	0.8	7.35	10	◇

to develop across the wire, and the critical current I_{c2} , where the resistivity reaches the normal-state resistivity, are measured in an He flow cryostat at different temperatures on a short segment, 1 cm long, of the wire using a dc four-probe measurement.

E. Bulk μSR

Standard μSR measurements of bulk $\text{La}_{1.94}\text{Sr}_{0.06}\text{CuO}_4$ powder were done on the GPS beamline at PSI with a standard He flow cryostat capable of cooling to 1.6 K. The same bulk sample was later used to prepare the wire. These measurements were used to determine the magnetic volume fraction and frozen moment size as discussed in Sec. III C.

III. RESULTS

A. Effect of current

Here we study the effect of the current on the magnetic order. Figure 3 shows raw muon decay asymmetry data from the meander wire at several temperatures with no external field. The open symbols represent measurements at low currents (used only for temperature determination) and the solid symbols are measurements at high currents. At $T > T_m$, the asymmetry resembles a Gaussian with relatively slow relaxation, typical of magnetic fields generated by copper nuclear magnetic moments. As the temperature decreases, there is a clear increase in the muon spin depolarization rate indicating that the magnetic order has set in.

The effect of the current is demonstrated by the $T=5$ K measurement (red squares in Fig. 3). The depolarization of the muons spin is faster when a higher current is applied. The difference between the two measurements is emphasized by the shaded area. The change in the asymmetry line shape caused by the application of current is equivalent to cooling by 0.3–0.4 K, although, as mentioned before, the sample temperature is stable to within 0.01 K. This effect was observed at several temperatures along the magnetic transition.

Above T_m and below 4 K the application of current has no effect on the asymmetry. This finding is particularly impor-

tant since, *a priori*, the current might affect the muon asymmetry directly by means of the magnetic field it produces, or by colliding with the muons. However, we found that once the electronic spins are fully frozen the current does not change the muon asymmetry indicating that there is no direct current muon coupling. This is in agreement with calculations showing that the magnetic field the current produces is very small compared to the internal field. Similarly, the lack of current effect above T_m rules out collisions between muon and electron charge.

In order to determine the magnetic phase transition temperature, without assuming a specific spatial field distribution or temporal fluctuation model, we define the order parameter in a model-free way. At each temperature the asymmetry as a function of time is averaged to produce $\langle \text{Asy} \rangle = \frac{1}{t_m} \int_0^{t_m} \text{Asy}(t) dt$, where the measurement time $t_m = 8 \mu\text{s}$. We expect $\langle \text{Asy} \rangle$ to decrease with increasing mag-

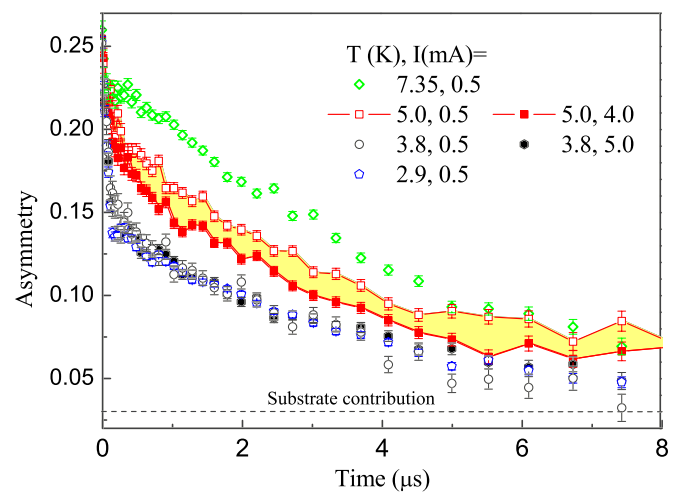


FIG. 3. (Color online) Muon decay asymmetry measurements versus time at low current (open symbols) and high current (solid symbols). Different colors and symbols represent different temperatures. The area shaded in yellow marks the effect of the current on the muon decay asymmetry at 5 K. The horizontal line shows the expected base line from the substrate.

netic moment size $M(T)$ and therefore defined

$$\frac{M(T)}{M(0)} \equiv \frac{\langle A_{sy} \rangle^{-1}(T) - \langle A_{sy} \rangle^{-1}(\infty)}{\langle A_{sy} \rangle^{-1}(0) - \langle A_{sy} \rangle^{-1}(\infty)}. \quad (2)$$

For $\langle A_{sy} \rangle(\infty)$ we take the averaged A_{sy} at $T=7.35$ K, which is above the transition. The magnetic phase transition temperature T_m is taken as the onset of the sudden change in $M(T)$. The magnetic transition is sharp enough that other, model-based, analysis methods gave indistinguishable $M(T)$. The temperature dependence of M with and without current is presented in Fig. 1.

We find that the application of a current of about $0.2I_{c2}(T)$ (see Sec. III D) increases the magnetic phase transition temperature by 0.4 ± 0.1 K. The fact that the current increases T_m and does not broaden the transition rules out the possibility of temperature inhomogeneities. As mentioned before, this effect means that the two orders interact repulsively. It is complementary to the effect of a strong magnetic field on doped samples, where the magnetic order is enhanced while the superconducting order is suppressed.^{9,10} However, since current, in contrast to magnetic field, does not couple directly to spins, the effect presented here is more simply analyzed. For example, it shows that the enhanced magnetism in the applied field could be a result of supercurrent in the bulk¹¹ and not necessarily due to magnetism in the vortex core.¹²

B. Superconducting properties

To determine the volume fraction of our sample we used transverse field of 1 kG measurements. Figure 4(a) depicts the results from the magnetic phase ($T=2.9$ K) in a rotating reference frame using zero-field cooling (ZFC). The muons depolarize very quickly and after $3 \mu\text{s}$ the remaining decay asymmetry is due to muons that have stopped in the substrate. For comparison, data from a blank substrate, normalized by its effective area, are also shown. We also present the decay asymmetry in the pure superconducting phase ($T=6$ K) using field-cooling conditions. In this case, the muon polarization is lost exponentially versus time at a rate r_{sc} due to the magnetic field distribution of the vortices in the superconducting phase. After $6 \mu\text{s}$ the polarization reaches the level of the substrate and the ZFC run, and thus most of the muons are affected by vortices.

We fit the function

$$A_{sy}(t) = A_{sc}e^{-(r_n t)^2/2 - r_{sc}t} \cos(\omega_{sc}t) + A_{sb}e^{-r_{sb}t} \cos(\omega_{n-sb}t) + A_n e^{-(r_n t)^2/2} \cos(\omega_{n-sb}t) \quad (3)$$

to the muon decay asymmetry at all temperatures. Here A_{sc} , A_{sb} , and A_n represent the respective contributions from the part of the meander that turns superconducting upon cooling, the substrate, and the part of the meander that remains normal upon cooling. r_{sc} , r_{sb} , and r_n are the relaxation rates of muons that land in a superconducting, substrate, and normal material, respectively. ω_{n-sb} is the rotation frequencies in the normal material and the substrate (taken to be equal). ω_{sc} is the rotation frequency in the superconducting part. The only parameters that are allowed to vary with T are r_{sc} and ω_{sc} . The superconducting volume fraction is estimated from $A_{sc}/(A_{sc}+A_n)$ and was found to be $90 \pm 5\%$.

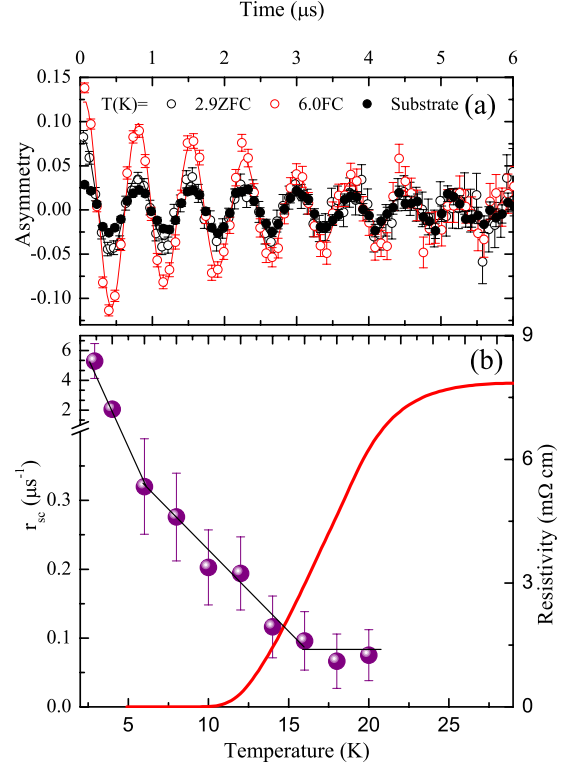


FIG. 4. (Color online) Determination of the superconducting volume fraction and penetration depth (a) μSR asymmetry under an applied field of 1 kG in a rotating reference frame at $T=2.9$ K with zero-field cooling, $T=6.0$ K with field cooling, and at $T=5$ K from the substrate. (b) The resistivity and muon depolarization rate r_{sc} as a function of temperature showing T_c . Below $T_m \approx 6$ K the muon relaxation increases rapidly.

Figure 4(b) shows r_{sc} and the resistivity versus temperature. The midpoint of the resistivity transition to the superconducting state and the onset of $r_{sc}(T)$ occur at $T_c=16$ K. The London penetration depth λ_{ab} at $T=7$ K is 500 nm as estimated from the relation $r_{sc}=0.04\gamma_\mu\phi_0/\lambda_{ab}^2$, where $\gamma_\mu/2\pi=13.5$ MHz/kG is the muon gyromagnetic ratio and ϕ_0 is the magnetic-flux quanta.¹³ This penetration depth value is similar to the meander thickness and therefore the current flows uniformly in the bulk of the meandering wire.

C. Magnetic volume fraction

We show in the Fig. 5 standard μSR measurements on the bulk powder used for making the film. In this case the measurements could be extended to $T=1.65$ K, much lower than in the LEM experiment. We find that the magnetic transition in the wire is very similar to that of ours and others bulk samples,^{1,5} having similar T_m . In addition, the data in the bulk at low enough temperatures are typical of the case where muons in the full sample volume experience frozen magnetism. When this happens 1/3 of the muons, on the average, experience a magnetic field in their initial spin direction. These muons do not depolarize. Therefore, at long time the asymmetry as a function of time is flat and near 1/3 of its initial value. If, in contrast, some of the muon do not experience frozen moments, they will have the same relax-

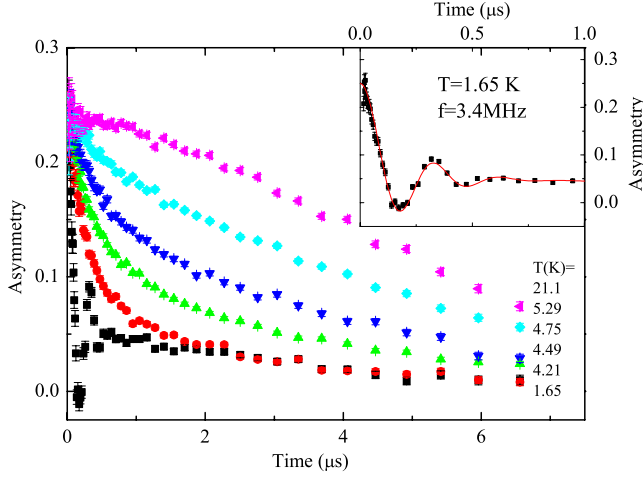


FIG. 5. (Color online) Standard μ SR measurements on the bulk powder used for making the film.

ation of the normal state. Our data shows a flat asymmetry at long time around 1/3 of the initial value with no observable relaxation. Therefore, all muons experience a frozen magnetic field and the magnetic volume fraction is 100%. Moreover, as demonstrated in the inset of Fig. 5, we find spontaneous precession below about 2 K. A fit of the data at $T = 1.65$ K to a Bessel-type relaxation function¹⁴ gives a frequency of $f \approx 3.4$ MHz. From the ratio of muon oscillation frequency between our sample and pure La_2CuO_4 (Ref. 15) and the magnetic moment of La_2CuO_4 (Ref. 16) we find an average local magnetic moment $M = 0.33\mu_B$ in our sample.

D. I_{c1} and I_{c2} determination

The V - I curves used for critical current determination are depicted in Fig. 6(a). They are fitted to the function $\Theta(I - I_{c1})e^{k(I - I_{c1})}$, where Θ is the Heaviside step function. It is seen in Fig. 6(a) that, at $T = 12$ K, I_{c1} drops to zero and the 1 cm segment of the wire shows Ohmic behavior with a normal resistance of $R_n = 60 \Omega$. We estimate I_{c2} using a variation in the offset criterion.¹⁷ The exponential dependence of V on I is extrapolated to the value of I that gives a differential resistance equal to 60Ω . The obtained values of both critical currents as a function of temperature are plotted in Fig. 6(b).

IV. DISCUSSION

A simple interpretation of the result can be given in the framework of the GL model. In this model the free-energy density near the critical temperature T_m can be written as

$$F = -a(T)(1 - I^2/I_{c2}^2)|\psi|^2 + U_s|\psi|^4 - b(T_m^0 - T)|\phi|^2 + U_m|\phi|^4 + 2U_{sm}|\phi|^2|\psi|^2, \quad (4)$$

(plus gradient terms) where ψ and $\phi = M/\sqrt{v}\mu_B$ are the superconducting and magnetic order parameters, respectively, U_{sm} is their coupling constant, v is the unit cell volume, b is a dimensionless parameter, T_m^0 is the magnetic phase transition temperature for $|\psi|^2 = 0$, $a(T)$, U_s and U_m are the stan-

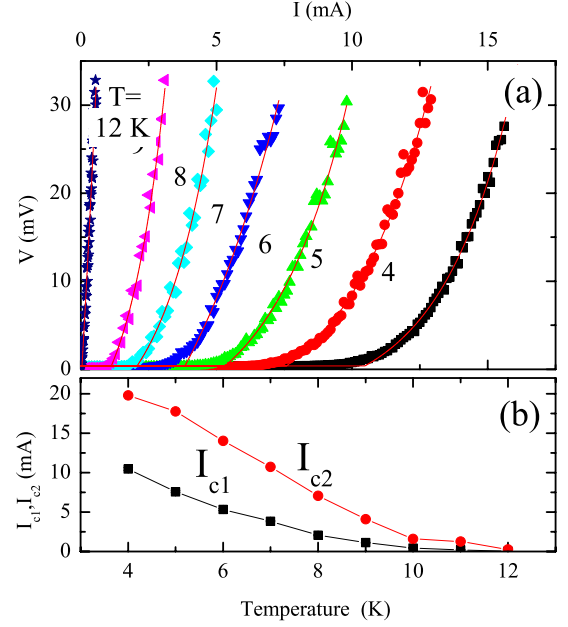


FIG. 6. (Color online) Calibration curves used for temperature determination and for the estimation of I_{c1} and I_{c2} . (a) V - I curves of a short segment of the wire. Similar measurements on the full wire are used for the temperature calibration. (b) I_{c1} and I_{c2} as a function of temperature were extracted from the data shown in the top panel.

dard GL parameters. All the parameters can be experimentally determined:^{18,19}

$$a(T) = \hbar^2/2m^*\xi^2,$$

where $\xi = 2$ nm is the superconducting coherence length,²⁰

$$\psi_0^2 = m^*/4\mu_0e^2\lambda^2,$$

where $\lambda = 500$ nm is the London penetration depth,

$$U_s = a/2\psi_0^2$$

according to the minimum condition,

$$bT_m = \hbar^2/2m\kappa^2,$$

where $\kappa = 4$ nm is the magnetic coherence length,^{21,22} the “magnetic” electron mass can be approximated by the stiffness of the xy model where

$$\hbar^2/mA = J,$$

A is the cell area, and $J \approx 10^3$ K is the superexchange. This electron mass is 1.6 larger than the free-electron mass, which could be used for our calculation equally well. Using the moment from Sec. III C we have $\phi_0^2 = 0.33^2/v$, and

$$U_m = bT_m/2\phi_0^2$$

again by the minimum condition.

U_{sm} is obtained from our current-dependent measurement (neglecting gradient terms at this stage). Since T_c is higher than T_m we do not expect $|\phi|^2$ to affect $|\psi|^2$. Therefore

$$|\psi(I, T)|^2 = |\psi(0, T)|^2(1 - I^2/I_{c2}^2). \quad (5)$$

The minimization of F with respect to $|\phi|^2$ yields,

$$|\phi|^2 = b[T_m^0 - 2U_{sm}|\psi(I, T)|^2/b - T]/2U_m. \quad (6)$$

Thus, the measured magnetic transition temperature is given by

$$T_m = T_m^0 - 2U_{sm}|\psi(I, T_m)|^2/b.$$

We assume that near T_m , $\psi^2(0, T) = \psi_0^2$, where ψ_0^2 is the ground-state value of ψ^2 . Therefore, the change in the transition temperature, $\delta T_m \equiv T_m(I) - T_m(0)$, caused by the current is

$$\delta T_m(I) = \frac{2U_{sm}\psi_0^2 I^2}{bI_{c2}^2}. \quad (7)$$

The interesting parameter is

$$R \equiv \frac{U_{sm}}{\sqrt{U_s U_m}} = \frac{2e\lambda\xi MI_{c2}^2 \delta T_m}{\mu_B \hbar \kappa I^2 T_m} \sqrt{\frac{J\mu_0}{h}}, \quad (8)$$

where h is the unit cell height. For $R > 1$ the GL model predicts phase separation and first-order phase transition between AFM and SC orders. For $R < 1$ the model predicts

coexistence and a second-order phase transition. The $R=1$ condition is essential for SO(5) symmetry.²³ At $T=5$ K we found that $I_{c2}=17$ mA [see Fig. 6(b)] and used $I=4$ mA in the LE- μ SR. This yields a positive $R=1.4$. Although numerical factors can change R , they cannot change its proximity to unity.

In summary, we demonstrated the presence of interaction between the magnetic and superconducting order parameters and measured its sign and strength. We find that phase transition at zero temperature from magnetic to superconducting orders, as a consequence of doping, must be very close to the boarder between first and second order.

ACKNOWLEDGMENTS

We acknowledge very helpful discussions with Assa Auerbach and Yariv Kafri. We also thank the PSI team for supporting the μ SR experiments and for providing the continuous high-quality beam. This work was also funded in part by the Israeli Science Foundation and the joint German-Israeli DIP project.

- ¹Ch. Niedermayer, C. Bernhard, T. Blasius, A. Golnik, A. Moodenbaugh, and J. I. Budnick, *Phys. Rev. Lett.* **80**, 3843 (1998).
- ²M.-H. Julien, F. Borsa, P. Carretta, M. Horvatic, C. Berthier, and C. T. Lin, *Phys. Rev. Lett.* **83**, 604 (1999).
- ³J. M. Tranquada, B. J. Sternlieb, J. D. Axe, Y. Nakamura, and S. Uchida, *Nature (London)* **375**, 561 (1995).
- ⁴C. Panagopoulos, J. L. Tallon, B. D. Rainford, T. Xiang, J. R. Cooper, and C. A. Scott, *Phys. Rev. B* **66**, 064501 (2002).
- ⁵B. J. Sternlieb, G. M. Luke, Y. J. Uemura, T. M. Riseman, J. H. Brewer, P. M. Gehring, K. Yamada, Y. Hidaka, T. Murakami, T. R. Thurston, and R. J. Birgeneau, *Phys. Rev. B* **41**, 8866 (1990).
- ⁶T. Prokscha, E. Morenzoni, K. Deiters, F. Foroughi, D. George, R. Kobler, A. Suter, and V. Vrankovic, *Nucl. Instrum. Methods Phys. Res. A* **595**, 317 (2008).
- ⁷E. Morenzoni, F. Kottmann, D. Maden, B. Matthias, M. Meyerberg, T. Prokscha, T. Wutzke, and U. Zimmermann, *Phys. Rev. Lett.* **72**, 2793 (1994).
- ⁸J. E. Sonier, *Rep. Prog. Phys.* **70**, 1717 (2007).
- ⁹S. Katano, M. Sato, K. Yamada, T. Suzuki, and T. Fukase, *Phys. Rev. B* **62**, R14677 (2000).
- ¹⁰B. Lake, H. M. Rønnow, N. B. Christensen, G. Aeppli, K. Lefmann, D. F. McMorrow, P. Vorderwisch, P. Smeibidl, N. Mangkorntong, T. Sasagawa, M. Nohara, H. Takagi, and T. E. Mason, *Nature (London)* **415**, 299 (2002).
- ¹¹E. Demler, S. Sachdev, and Y. Zhang, *Phys. Rev. Lett.* **87**, 067202 (2001).
- ¹²J.-P. Hu and S.-C. Zhang, *J. Phys. Chem. Solids* **63**, 2277 (2002).
- ¹³E. H. Brandt, *Phys. Rev. B* **37**, 2349 (1988).

- ¹⁴A. T. Savici, Y. Fudamoto, I. M. Gat, T. Ito, M. I. Larkin, Y. J. Uemura, G. M. Luke, K. M. Kojima, Y. S. Lee, M. A. Kastner, R. J. Birgeneau, and K. Yamada, *Phys. Rev. B* **66**, 014524 (2002).
- ¹⁵Y. J. Uemura, W. J. Kossler, X. H. Yu, J. R. Kempton, H. E. Schone, D. Opie, C. E. Stronach, D. C. Johnston, M. S. Alvarez, and D. P. Goshorn, *Phys. Rev. Lett.* **59**, 1045 (1987).
- ¹⁶Y. S. Lee, R. J. Birgeneau, M. A. Kastner, Y. Endoh, S. Wakimoto, K. Yamada, R. W. Erwin, S.-H. Lee, and G. Shirane, *Phys. Rev. B* **60**, 3643 (1999).
- ¹⁷J. W. Ekin, in *Concise Encyclopedia of Magnetic and Superconducting Materials*, edited by J. E. Evetts (Pergamon, New York, 1991).
- ¹⁸K. Huang, *Statistical Mechanics*, 2nd ed. (John Wiley & Sons, New York, 1987), p. 425.
- ¹⁹P. G. de Gennes, *Superconductivity of Metals and Alloys* (Westview Press, Boulder, Colorado, 1999), p. 185.
- ²⁰H. H. Wen, H. P. Yang, S. L. Li, X. H. Zeng, A. A. Soukiassian, W. D. Si, and X. X. Xi, *Europhys. Lett.* **64**, 790 (2003).
- ²¹R. J. Birgeneau, D. R. Gabbe, H. P. Jenssen, M. A. Kastner, P. J. Picone, T. R. Thurston, G. Shirane, Y. Endoh, M. Sato, K. Yamada, Y. Hidaka, M. Oda, Y. Enomoto, M. Suzuki, and T. Murakami, *Phys. Rev. B* **38**, 6614 (1988).
- ²²B. Keimer, N. Belk, R. J. Birgeneau, A. Cassanho, C. Y. Chen, M. Greven, M. A. Kastner, A. Aharony, Y. Endoh, R. W. Erwin, and G. Shirane, *Phys. Rev. B* **46**, 14034 (1992).
- ²³E. Demler, W. Hanke, and S. C. Zhang, *Rev. Mod. Phys.* **76**, 909 (2004).